ARTICLE NO. 79-0652R

C80-029

Some Effects of Applying Sonic Boom Minimization to Supersonic Cruise Aircraft Design

00006
20001
20005

Robert J. Mack* and Christine M. Darden*
NASA Langley Research Center, Hampton, Va.

This paper presents a discussion of an aircraft shaping method to control sonic boom overpressure levels along with the analysis of wind tunnel data which validated the method. The results indicate that the sonic boom minimization method can guide the design team choices of aircraft planform and component arrangement toward a low-boom-level configuration while permitting sufficient freedom and flexibility to satisfy other design criteria. Further, it is shown that off-design flight conditions do not drastically change the overpressure sonic boom shape and strength.

Nomenclature

A_e = effective area
F = Whitham "F-function"
h = altitude
K_R = sonic boom reflection factor
ℓ = longitudinal length
M = Mach number
Δp = incremental pressure in flowfield of model
p = freestream static pressure
W_c = aircraft weight in cruise
ΔX = increment in x-direction
X = distance along the streamwise axis
α = angle of attack
β = $\sqrt{M^2-1}$
λ = "spike" width fraction of the F-function length
Λ = leading-edge sweep angle

Subscripts

D = design condition
e = effective value
NS = nose shock
TS = tail shock

Introduction

UNDER present regulations, commercial supersonic transport aircraft are permitted to cruise at supersonic speeds only over water or nonpopulated land routes. If future regulations were to define both acceptable and attainable sonic boom levels, a sizeable and potentially profitable market for next-generation supersonic cruise aircraft would open.

The sonic boom technology which will aid in building the aircraft for this possible future market is beginning to emerge from the research of the past and present. Analytical methods are being developed which permit sonic boom constraints to be included with the usual aerodynamic, structural, propulsion, etc., criteria. This paper discusses an aircraft shaping method for minimizing the ground level sonic boom and presents some experimental results which validate it. Unique design features of the wind-tunnel models are noted insofar as they are affected by these sonic boom constraints.

Background of Minimization Method

The sonic boom minimization method used in the study evolved from many contributions during the past 25 years. Whitham derived the original sonic boom theory[1] using a body-shape-related "F-function" to obtain a pressure signature in the flowfield about a body of revolution. Walkden[2] extended this theory to winged lifting bodies at far-field distances.

Jones[3] tailored the F-function to obtain a far-field minimum impulse pessure signature with the familiar N-wave shape. McLean's study[4] of pressure signature characteristics led to the hypothesis that near-field signature features probably persist from the aircraft to the ground during the transonic acceleration phase of supersonic cruise aircraft flight. Hayes[5] extended McLean's idea by showing that real atmosphere effects tend to "freeze" the signature shape well before the disturbances reach the ground from cruise flight altitude. Seebass and and George[6] combined these ideas into an isothermal atmosphere sonic boom prediction method which minimizes either the overpressure or the nose shock for a signature which retains near-field features. Darden[7] modified the Seebass and George method to account for standard atmosphere effects and developed a computer code[8] which permitted control of the required nose blunting. Carlson[9] applied this minimization method to several conceptual aircraft and showed, theoretically, that appreciable reduction in the ground level sonic boom could be obtained. The favorable results of Carlson's theoretical study gave impetus to a wind-tunnel test program for validating the boom minimization method.[10] Data from this wind-tunnel study are presented and discussed in this paper.

Implementation of Design Process

Figure 1 presents an outline of this minimization method and shows the required design condition input parameters. The F-function and the ground level pressure signature are shown for the two options of minimizing either overpressure or nose shock. Neither the nose shock Δp nor the overpressure Δp are program inputs; they are determined by calculation. Lengthy iterations are avoided by using the results of Ref. 8 which indicate how Δp can vary with typical input parameters. For aircraft shaping, the minimization method produces only an effective area distribution, A_e, which includes both aircraft volume and lift contributions.

Figure 2 shows two significantly different aircraft models which satisfy the same design conditions, have the same

Presented as Paper 79-0652 at the AIAA 5th Aeroacoustics Conference, Seattle, Wash., March 12-14, 1979; submitted April 2, 1979; revision received Aug. 31, 1979. Reprints of this article may be ordered from AIAA Special Publications, 1290 Avenue of the Americas, New York, N.Y. 10019. Order by Article No. at top of page. Member price $2.00 each, nonmember, $3.00 each. **Remittance must accompany order.**

Index categories: Configuration Design; Aeroacoustics; Computational Methods.

*Aerospace Technologist, Supersonic Aerodynamics Branch, High-Speed Aerodynamics Division. Member AIAA.

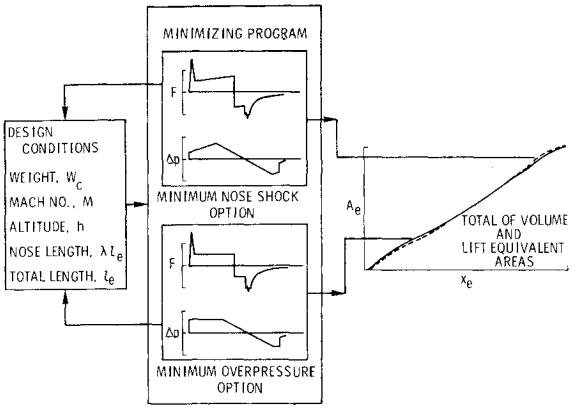

Fig. 1 Outline of minimizing procedure.

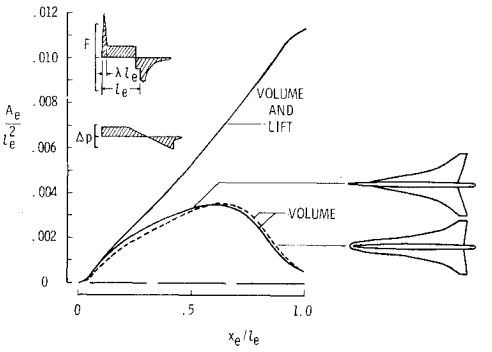

Fig. 2 Examples of design procedure.

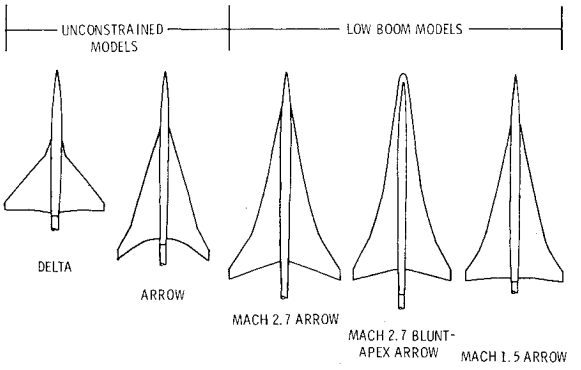

Fig. 3 Models used in sonic boom minimization study.

"spiked" F-function, and produce the same minimum overpressure sonic boom. The most noticeable differences are the wing planforms and the effective area distributions of the volume and the lift. Obviously, there is no unique aircraft shape; other configurations can be designed to meet the same cruise flight conditions and still produce the same minimum overpressure signature. This is possible because both the lift and the volume can be combined in a variety of ways to satisfy both the sonic boom constraints and the aerodynamic, structural, propulsion, etc., requirements.

Since the width of the F-function spike, λ, is variable, drag boom trade-off studies can be made early in the preliminary design stage. Reference 8 shows some estimated drag reductions that could come from lengthening the nose spike. The two configurations seen in Fig. 2 could be used to study the effects of wave drag, drag-due-to-lift, weight, and sonic boom by varying the value of λ and changing the nose contours. These studies would, of course, be entirely theoretical, but valuable data and significant trends could be highlighted for use in the design development. Thus, considerable freedom and flexibility is inherent in the method.

Description of Wind-Tunnel Models

The five models used in the wind tunnel study are shown in Fig. 3. The unconstrained delta and arrow wing models served as reference models. They were obtained from Ref. 9 in which similar aircraft were used to represent state-of-the-art technology and high supersonic aerodynamic efficiency technology. The other three models were designed with the minimum overpressure option of the minimization program. They had these full-scale aircraft design conditions in common:

W_c $= 600{,}000$ lb

ℓ $= \ell_e = 300$ ft

λ $= 0.1$

K_R $= 1.9$

sea level ΔP_{NS} $= \Delta P_{TS} \leq 1.0$ lb/ft^2 (approximate)

Two of the three low-boom models were designed for cruise at Mach 2.7 and an altitude of 60,000 ft, while the third was designed for cruise at Mach 1.5 and 50,000 ft. A Mach number of 2.7 was used in the early supersonic transport feasibility studies and is approaching the upper limits of the near-field sonic boom theory. Mach 1.5 was judged to be near the lower limit for supersonic cruise aircraft and is where linearized theory is accepted as valid for slender bodies.

The models were simple wing-body configurations with only the basic volume and lift contributing to the effective areas. The wing panels were planar with symmetrical airfoils and sharp leading and trailing edges. Circular section fuselages were faired around the root chord and blended into the sting support. Boundary-layer displacement thickness effects were assumed to be small and were not included in the configuration designs; this significantly reduced the time and iterations required to obtain a good match between the boom constrained and the configuration effective area curves. However, these boundary layer effects were found to be significant and will be discussed later.

The three low-boom models seen in Fig. 3 had several common design features which are shown in Fig. 4. All three were given low aspect ratio arrow wing planforms to provide the length required for a gradual, controlled lift and volume development. Wing dihedral was used to maintain a full-scale effective length of 300 ft. The inboard wing panels were highly swept, $\beta \cot \Lambda < 1$, to control the lift and volume contribution growth behind the nose section. However, a supersonic leading edge, $\beta \cot \Lambda > 1$, was used on the outboard wing panel (of the Mach 2.7 aircraft) to obtain reasonable full-scale aircraft wing spans in the range of 140-160 ft. This produced wing areas of 15,000 ft^2 or more. Since the angles of attack needed to obtain the required lift were in the 2-4 deg range, these aircraft were small disturbance bodies, in the linearized theory sense.

Wing thickness ratios were varied across the semispans to achieve reasonable wing volumes. Fuselages were given sufficient volume for sting attachment strength and were modified, along with the wing thickness, to obtain the area-rule fine tuning to match the effective area curve with the minimum boom constraint curve.

The Mach 2.7 arrow and the Mach 1.5 arrow wing models were designed with the required nose blunting supplied by volume contribution alone; thus, they were very similar in overall appearance despite the difference in design Mach number. For the Mach 2.7 blunt-apex arrow wing model, both lift and volume contributions were employed to meet the nose bluntness requirement. The effects of this alternate design approach can be seen in Figs. 2 and 3. With the wing

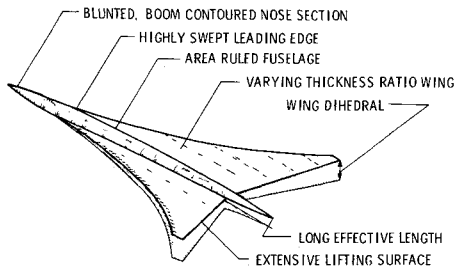

Fig. 4 Features of low-boom models.

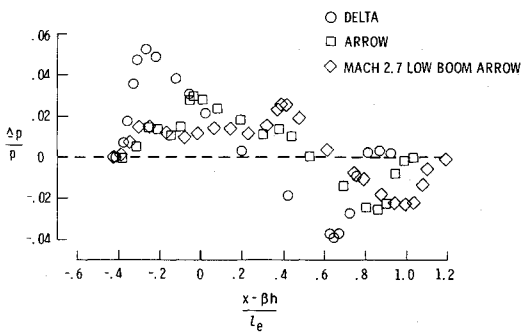

Fig. 5 Measured pressure signatures of unconstrained delta, unconstrained arrow, and Mach 2.7 low-boom arrow wing models at $M = 2.7$ and $h/\ell_e = 3$.

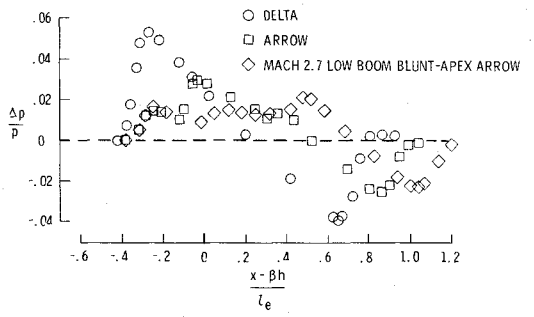

Fig. 6 Measured pressure signatures of unconstrained delta, unconstrained arrow, and Mach 2.7 low-boom, blunt apex arrow wing models at $M = 2.7$ and $h/\ell_e = 3$.

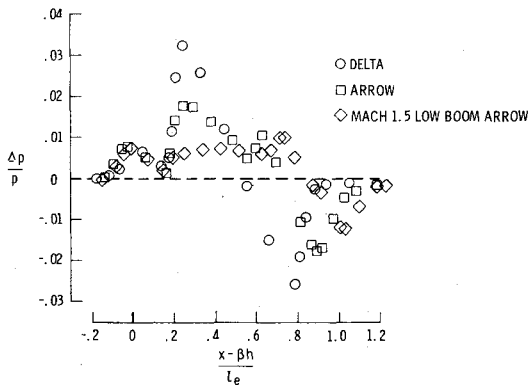

Fig. 7 Measured pressure signatures of unconstrained delta, unconstrained arrow, and Mach 1.5 low-boom arrow wing models at $M = 1.5$ and $h/\ell_e = 3$.

apex beginning at the configuration nose, lift and thickness contributions start early and combine quickly to change the shape of the aircraft nose section markedly. The fuselage maximum diameter is 18% less than that of the Mach 2.7 arrow wing aircraft model because fuselage volume has been replaced with wing thickness volume and lift effective area contributions. However, to keep the wing area about the same on all the low-boom models, the wing span of the blunt arrow was reduced from 160 to 140 ft. This, in turn, required more wing dihedral to keep the effective length constant at 300 ft.

These design features, which are summarized in Fig. 4, were applied throughout the iteration process to obtain the desired total effective area distribution. After each geometry modification, wing planform, wing thickness, and fuselage thickness descriptions provided inputs to a wing analysis computer program[11] and a wave-drag area-rule computer program[12] which had been modified to obtain both lift and volume effective area contributions. Comparison of design and boom constrained effective area curves showed where adjustments in planform shape, wing thickness, and/or fuselage volume were needed to obtain a good match. When a satisfactory solution was obtained, a 1/600th scale (6 in.) wind-tunnel model was built from the design.

Presentation and Analysis of Experimental Results

The models were tested in the Unitary Plan wind tunnel using the procedures outlined in Ref. 10. Pressure signatures were measured at Mach numbers of 1.5, 2.6, 2.7, and 2.8, at angle of attack to design angle-of-attack ratios of 0.8, 1.0, and 1.2, and at a distance of 18 in. (three low-boom model lengths) below the flight path.

Configuration Effects

Figures 5-7 show the measured pressure signatures of the three low-boom models along with signatures of the reference models at conditions of design Mach number and an angle of attack that would produce a full-scale lift of 600,000 lb. In all three figures, marked differences in signatures are clearly seen for this near-field location.

At Mach 2.7 (Figs. 5 and 6), the delta wing model produces an N-wave signature. Nose bluntness and rapid lift buildup combine to force rapid coalescence of the individual nose and wing shocks. The delta wing nose overpressure peak has three times the strength of the nose shocks from the unconstrained arrow and low-boom arrow wing models and twice the strength of the maximum overpressure on the unconstrained arrow wing model signature.

In contrast to the delta wing, noticeable near-field characteristics are evident on the unconstrained arrow wing model signature. Although the peak pressure level of the wing shock is about twice that of the nose shock, the wing shock strength (pressure jump) is only about 30% larger than the nose shock strength.

As theoretically predicted, both low-boom models of Figs. 5 and 6 exhibit signatures having moderate nose shocks followed by a pressure plateau absent of discrete wing shocks. Although the pressure rise preceding the final expansion is due mainly to the boundary layer growth, there is probably a contributing increment due to the local increase in effective lift development as the wing leading edge changes from subsonic to supersonic (Ref. 2). This effect is more noticeable in Fig. 5 because the value of $\beta \cot \Lambda$ was 1.54 as compared to 1.25 on the model whose pressure signatures is seen in Fig. 6.

Figure 7 presents Mach 1.5 data in which near-field signature characteristics are evident for all three models. Each signature has similar shape and strength nose shocks, but the wing compressions differ considerably. The delta wing model signature exhibits wing induced shock pressure levels four times as large as the nose shock and the basic arrow wing shock pressures are about twice that of the nose shock. The low-boom model design successfully suppressed the wing shocks and nowhere does the pressure significantly exceed nose shock levels. As previously observed at Mach 2.7, the low-boom model signature exhibited an unexpected pressure rise slightly ahead of the expansion; this pressure rise can be related mainly to boundary-layer effects since the leading edge is subsonic from root to tip.

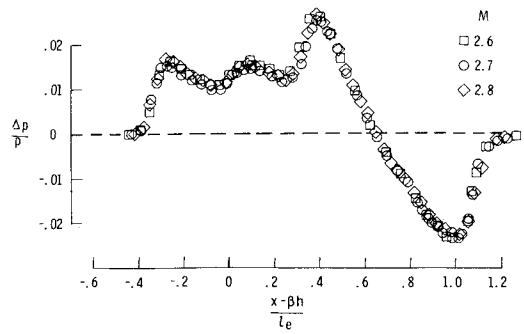

Fig. 8 Signature sensitivity with Mach number of Mach 2.7 low-boom arrow wing model at $\alpha/\alpha_D = 1$.

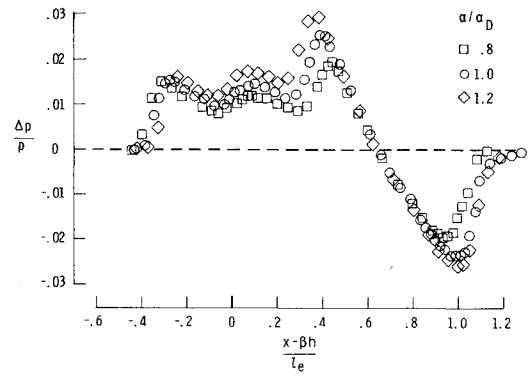

Fig. 9 Signature sensitivity with angle-of-attack of Mach 2.7 low-boom arrow wing model at $M = 2.7$.

The importance of these near-field characteristics is in the signature development as it propagates from the aircraft to the ground. In general, the signature shape will undergo changes during midfield propagation and then will propagate unchanged or frozen through the remainder of the field. During the initial propagation phase, the near-field features of the basic delta and arrow will most likely develop into an N-wave due to the coalescence of the bow and wing shocks; the shock formed by this coalescence can be three to four times larger than the near-field bow shock. The low-boom model signatures do not have a wing shock to coalesce with the bow shock and would not be expected to form an N-wave during the initial phase of propagation; the near-field features would remain through the entire field of propagation resulting in ground pressure signatures of the near-field shape with attenuated bow shock levels.

Some other general observations can be deduced from the data of Figs. 5-7. Nose shock or peak overpressure strength can be seen to decrease noticeably as signature length increases. Similar trends are found with the impulse (integral of the positive pressures). These benefits are due to the more gradual lift development and to the controlled buildup of both the volume and lift effective areas.

Mach Number and Angle of Attack Effects

The sensitivity of pressure shape and strength to changes in Mach number and angle of attack (cruise weight) is seen in Figs. 8 and 9. It is shown for the Mach 2.7 low-boom arrow wing model since similar results were measured for the other low-boom models.

At $\alpha/\alpha_D = 1.0$, nose shock strength and signature length are virtually unaffected by a ± 0.1 change in freestream Mach number. Since angle of attack spans a ± 0.1 range at Mach 2.7, the signature differences are much more obvious. The impulse and the maximum overpressure vary almost linearly with angle of attack although the nose shock strength remains almost constant. These differences are more pronounced than if both Mach number and angle varied by the same ratio.

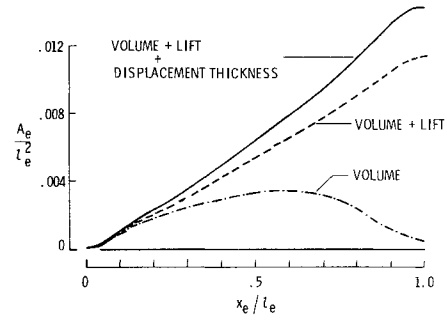

Fig. 10 Method for including viscous effects on Mach 2.7 low-boom arrow wing model at $M = 2.7$.

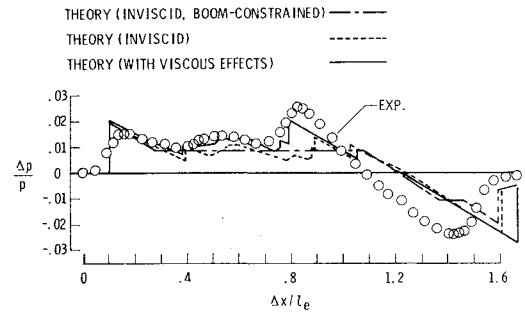

Fig. 11 Comparison of measured and theoretical signatures for Mach 2.7 low-boom arrow wing model at $M = 2.7$ and $h/\ell_e = 3$.

Therefore, flight Mach number and angle of attack could vary from design conditions by a few percent without causing noticeable increases in either nearfield or ground overpressures.

Effects of Boundary Layer and Model Inaccuracies

Definite flat-top characteristics are seen in the low-boom model pressure signatures (Figs. 5-9), although they are masked by unexpected waves and peaks. These effects are caused by model design and construction inaccuracies, and boundary layer effects. The first cause is very difficult to avoid on such small models; however, theoretical assessments of model construction inaccuracies can be made by carefully measuring the wind-tunnel model and computing signatures for the measured model geometry. Likewise, the boundary layer effects can be assessed by adding computed displacement thicknesses to the measured model geometry and calculating signatures.

The method for including viscous effects in the sonic boom prediction procedure is illustrated in Fig. 10 for the Mach 2.7 low-boom arrow wing model. The effective area due to volume was obtained from measured model geometry, and the effective area due to lift was obtained by the method previously discussed. Incremental cross-sectional areas produced by displacement thickness were calculated by the method of Ref. 13 and added to the volume and lift areas. At the most aft position $x_e/\ell_e = 1.0$, displacement thickness increased the total effective area by 20%.

In order to demonstrate the effects of model design and construction inaccuracies and displacement thickness effects, three theoretical signatures were calculated and compared with experimental data for each of the low-boom models in Figs. 11-13. The "inviscid, boom-constrained" signature represents the goal as specified by the minimization method; the "inviscid" signature is obtained from measured model geometry; and the "with viscous effects" signature includes the effective area increment due to displacement thickness.

At Mach 2.7, the signatures using theory (with viscous effects) are in reasonably good agreement with measured signatures over the positive overpressure part of the signature;

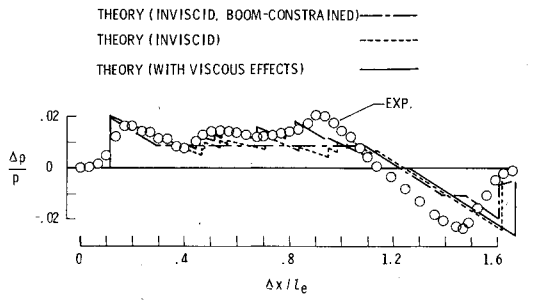

Fig. 12 Comparison of measured and theoretical signatures for Mach 2.7 low-boom blunt apex arrow wing model at $M=2.7$ and $h/\ell_e=3$.

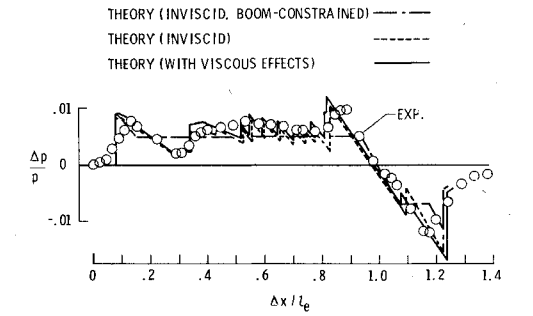

Fig. 13 Comparison of measured and theoretical signatures for Mach 1.5 low-boom arrow wing model at $M=1.5$ and $h/\ell_e=3$.

however, at Mach 1.5, the agreement between the inviscid theory signature, the viscous corrected signature, and the measured signature is good over all of the signature. This kind of disagreement between the predicted and the measured signature of winged lifting bodies at the higher Mach numbers has been reported before (Ref. 14-16).

The difficulties faced in designing and building sonic boom wind-tunnel models can be seen by comparing the boom-constrained and wind-tunnel model inviscid theory signatures. Small differences between the actual and the desired effective area curves appear as waves which are somewhat accentuated by additional inaccuracies introduced during model construction.

Problems also arise from viscous scaling effects when small wind-tunnel models are used to assess the sonic boom generated by full-scale aircraft. These problems come primarily from the dissimilar natures of the boundary layers on the full-scale aircraft at flight conditions and on the wind--tunnel models at wind-tunnel test conditions.

One method of addressing this problem was used in the wind-tunnel study of Ref. 10. The models were designed with inviscid theory, and the net effective area due to model volume and lift was corrected by adding displacement thickness effective area before calculating the theoretical pressure signatures.

Another method for including viscous effects is to calculate displacement thickness effective area concurrently with volume and lift effective areas at each design iteration and use the sum of these three effective areas as an input for an updated minimum-boom constraint curve. While the second method is more exact, the first was considered adequate for the present investigation. However, test results demonstrated that methods for including boundary layer effects need further study and development.

It can be concluded that most of the disagreement initially encountered between theoretically predicted and measured pressure signatures can be resolved by properly accounting for small differences in the design and the desired boom-constrained effective area curves, small inaccuracies which occur in model construction and boundary-layer displacement thickness on sonic boom models. The portion of the signature for which good agreement between the theory and experiment exists decreases as the Mach number exceeds 2.0; but even at Mach 2.7, sufficient agreement between theoretical and experimental pressure signatures was obtained to validate the sonic boom minimization method.

Conclusion

The results of an experimental study which tested the validity and applicability of a sonic boom minimization method have been reported along with a brief discussion of its influence on the design of low-boom aircraft models. During the discussion and analysis, several points were noted as significant conclusions:

1) The sonic boom minimization method is valid and applicable to the design of low-boom supersonic cruise aircraft.

2) The method has inherent flexibility which can be used to satisfy other aircraft design criteria.

3) Low-boom model pressure signatures are relatively insensitive to small variations from design Mach number and angle of attack.

4) Boundary-layer displacement thickness effects are significant on small-scale sonic boom models, and including these effects significantly improves the agreement between measured and predicted pressure signatures.

References

[1] Whitham, G.B., "The Flow Pattern of a Supersonic Projectile," *Communications in Pure and Applied Mathematics*, Vol. V, August 1952, pp. 301-348.

[2] Walkden, F., "The Shock Pattern of a Wing-Body Combination Far From the Flight Path," *Aeronautical Quarterly*, Vol. 9, May 1958, pp. 164-194.

[3] Jones, L.B., "Lower Bounds for Sonic Bangs," *Journal of the Royal Aeronautical Society*, Vol. 65, June 1951, pp. 433-436.

[4] McLean, F.E., "Some Nonasymptotic Effects on Sonic Booms of Large Airplanes," NASA TN D-2877, 1965.

[5] Hayes, W.D., Haefeli, R.C., and Kulsrud, H.E., "Sonic Boom Propagation in a Stratified Atmosphere, With Computer Program," NASA CR-1299, 1969.

[6] Seebass, R. and George, A.R., "Sonic Boom Minimization," *Journal of Acoustical Society of America*, Vol. 51, pt. 3, Feb. 1972, pp. 686-694.

[7] Darden, C.M., "Minimization of Sonic Boom Parameters in Real and Isothermal Atmospheres," NASA TN D-7842, 1975.

[8] Darden, C.M., "Sonic Boom Minimization With Nose Bluntness Relaxation," NASA TP 1348, 1979.

[9] Carlson, G.W., Barger, R.L., and Mack, R.J., "Application of Sonic Boom Minimization Concepts in Supersonic Transport Design," NASA TN D-7218, 1973.

[10] Mack, R.J. and Darden, C.M., "A Wind-Tunnel Investigation of the Validity of a Sonic Boom Minimization Concept," NASA TP 1421, 1979.

[11] Carlson, H.W. and Miller, D.S., "Numerical Methods for the Design and Analysis of Wings at Supersonic Speeds," NASA TN D-7713, 1974.

[12] Harris, R.V., Jr., "A Numerical Technique for Analysis of Wave Drag at Lifting Conditions," NASA TN D-3586, 1966.

[13] Monaghan, R.J., "An Approximate Solution of the Compressible Laminar Boundary Layer on a Flat Plate," R. and M. No. 2760, Brit. A.R.C., 1953.

[14] Miller, D.S., Morris, O.A., and Carlson, H.W., "Wind-Tunnel Investigation of Two Simple Wing Models at Mach Numbers From 2.3 to 4.63," NASA TN D-6201, 1971.

[15] Carlson, H.W., McLean, F.E., and Shrout, B.L., "A Wind-Tunnel Study of Sonic-Boom Characteristics for Basic and Modified Models of a Supersonic Transport Configuration," NASA TM X-1236, 1966.

[16] Morris, O.A., Lamb, M., and Carlson, H.W., "Sonic-Boom Characteristics in the Extreme Near Field on a Complex Airplane Model at Mach Numbers of 1.5, 1.8, and 2.5," NASA TN D-5755, 1970.